Redistribution of Residual Stress by Thermal Shock in Reactor Pressure Vessel Steel Clad With Nickel Alloy

Sam Oliver, Mahmoud Mostafavi, Foroogh Hosseinzadeh, Martyn Pavier

Abstract

This paper characterises the residual stress in nuclear reactor pressure vessel steel clad with nickel-based alloy and investigates the interaction between residual and thermal stresses during thermal shock. Residual stress measurements were made on two plates of SA508 Grade 4N steel, clad with Alloy 82 nickel-based alloy. The techniques used to measure the residual stresses were: deep hole drilling, centre hole drilling, and the contour method. One plate was as-welded, the other post-weld heat-treated. The post-weld heat-treated plate was subjected to thermal shock by heating it up and then spraying the surface of the cladding with cold water. The residual stress was measured again afterwards. A finite element simulation was made to investigate the physical mechanisms causing residual stress redistribution during thermal shock. Thermal shock caused significant residual stress redistribution in the cladding due to elastic-plastic interaction between the thermal stress and the cladding residual stress. The results demonstrate that an assessment of the safety of a reactor pressure vessel during thermal shock could be conservative for small surface defects if it is assumed that residual and thermal stresses combine elastically.

Keywords: Residual stress, thermal stress, thermal shock, cladding, structural integrity.

1 Introduction

The reactor pressure vessel (RPV) in a pressurised water reactor is clad on its internal surface for improved corrosion resistance, traditionally by weld overlaying with stainless steel, although more recently nickel-based alloys have been investigated as an alternative cladding material. The cladding process introduces residual stresses, and it is important to understand how these stresses combine with other loads to contribute to failure. One particularly severe loading scenario that an RPV must be able to withstand occurs under fault conditions when there is a loss of primary coolant, for example caused by a break in a pipe. Emergency cooling water is injected into the hot reactor to replace the missing primary coolant. The effect is to rapidly cool the internal surface of the vessel whilst the bulk of the material remains at high temperature. The resulting thermal mismatch causes large tensile stresses at the internal (clad) surface, a scenario known as thermal shock [1]. The RPV may still contain pressure during some fault conditions, but this work only considers a severe case in which the pressure rapidly drops to zero due to a large break in a pipe.

Accurately assessing the integrity of an RPV subjected to thermal shock requires knowledge of the thermal stress and cladding residual stress, and an understanding of how they combine to cause a defect to propagate. After cladding, RPVs are usually subjected to post-weld heat-treatment, whereby the material is maintained at high temperature to partially relax the residual stress by creep [2]. However, the residual stress is not completely erased [2-4] because additional stresses are generated upon cooling due to the difference in thermal expansion coefficient between the cladding and parent materials. The residual stress in pressure vessel steel clad with stainless steel has been well characterised in previous work using modelling techniques [2, 4] and experimental measurements [2-10]. In general, material which has been post-weld heat-treated contains high tensile residual stress in the cladding of around 200 – 400 MPa, and lower-magnitude tensile or compressive stress in the parent [3, 7, 11]. The number of residual stress measurements reported in the open literature on nickel-alloy cladding is comparatively limited. One study [6] reported measurements on various pieces of low-alloy steel clad with Alloy 600 nickel-based alloy. In one piece extracted from a spherical section of a pressure vessel, up to 255 MPa tensile stress was measured in the cladding. Thermal shock stresses are also tensile in the cladding, and of high magnitude. Calculations in previous work suggest the magnitude of thermal shock stress alone can be up to 900 MPa if the material is assumed linear-elastic [12, 13].

It has been demonstrated that thermal shock stress and cladding residual stress are both tensile at the inner wall of the RPV in the cladding, and of high-magnitude. An understanding of how these two sources of stress combine is required to accurately assess the integrity of an RPV containing a defect, particularly for surface defects which may arise due to stress corrosion cracking. Current guidance in Section II.6.8 of R6 [14], a structural integrity assessment procedure widely used in the nuclear industry in the UK, gives the following calculation for the total stress intensity factor, K_{tot}, when the combined thermal and residual stresses exceed the yield strength:

$$K_{tot} = K_J^{th} + K_{RS} \quad (1)$$

where K_J^{th} is the stress intensity factor due to thermal stress calculated using elastic-plastic analysis, and K_{RS} is the linear-elastic stress intensity factor due to residual stress. Equation (1) assumes that the elastic-plastic thermal shock stresses and the elastic residual stresses combine elastically. Using upper-bound values from the literature of 400 MPa for the elastic-plastic thermal shock stresses [12] and 400 MPa for the cladding residual stresses [7], the elastically combined stress is 800 MPa, which is well in excess of the yield strength of typical cladding material (268 - 299 MPa for unirradiated stainless steel cladding at room temperature [15]). This implies that combining thermal and residual stresses during thermal shock using elastic superposition, for example with Equation (1), could be overly-conservative, particularly for short defects which exist mostly under tensile stress in the cladding. Inelastic interaction between residual stress and mechanical load has been previously demonstrated by measuring residual stress before and after mechanical loading [16, 17]. In the NESC-1 spinning cylinder experiment [18], residual stress measurements were carried out on an RPV mock-up before and after it was subjected to thermal shock, although this study included internal pressure, and

it is therefore not clear whether residual stress redistribution occurred due to interaction with thermal load, pressure load, or a combination of the two.

This work has two objectives. The first objective is to measure the residual stress in SA508 Grade 4N, a modern nuclear pressure vessel steel, clad with Alloy 82 nickel-based alloy. This will provide important data on residual stress in nickel-clad RPVs, on which there are currently very few measurements reported in the open literature. The second objective is to investigate whether the cladding residual stress redistributes during thermal shock. This will be achieved experimentally, by subjecting the clad material to thermal shock and then re-measuring the residual stress, and also numerically using finite element modelling. It is expected that significant residual stress redistribution occurs during thermal shock, which would provide experimental validation to the prediction that combining the residual and thermal stresses by elastic superposition is overly-conservative. Measurements of residual stress after thermal shock will also allow better judgement of the structural integrity of an RPV when re-entering service after a fault.

2 Experimental method

2.1 Materials

Figure 1 shows a schematic of the two clad plates obtained for this work. In both plates, the parent material is SA508 Grade 4N, a modern high-strength nuclear pressure vessel steel, and the cladding is Alloy 82, a nickel-based alloy. The cladding was deposited by overlay welding. One plate is in the as-welded condition, and one has been post-weld heat-treated. The as-welded plate is clad on two opposite sides, each side with two layers of weld. The weld bead is laid in the same direction on both sides. Note that RPVs are usually only clad on a single side (the internal surface), but single-side clad material in the as-welded condition was unavailable for this project. The post-weld heat-treated plate is clad on a single side with three layers of weld. The weld bead is laid in a different direction on each half of the plate. The cladding on both plates has been machined down to a uniform thickness using face milling. The cutter travelled in the x_1 direction on both plates, referring to the co-ordinate system in Figure 1. The thickness of the cladding as shown in Figure 1 is nominally 4.25 mm on each side of the as-welded plate and 6 mm on the post-weld heat-treated plate, although in practice the cladding is slightly thicker on both plates due to melting and redistribution of material during welding.

2.2 Cladding tensile tests

Room temperature tensile tests were carried out on the cladding material to determine material properties for finite element modelling and residual stress measurements. Four specimens were extracted from the cladding on one side of the as-welded block using wire electro-discharge machining. Two were aligned longitudinally to the weld direction, and two were transverse. The specimens were rectangular and their geometries conformed to ASTM E8/E8M [19], where the longitudinal specimens were subsize (25 mm gauge length) and the transverse specimens were sheet-type (50 mm gauge length). All specimens were 3.4 mm thick and contained only cladding. Tests were carried out in displacement control at 20°C. The specimen extension was measured using extensometers. The measured value of Young's modulus was 172.4 GPa, calculated as the average of several load-unload cycles on two specimens (one in each orientation) up to a maximum of 0.07% strain. The maximum value from all tests was 175 GPa and the minimum was 162 GPa. The two remaining specimens were tested to failure. The engineering stress-strain curve of the transverse specimen is shown in Figure 2. The 0.2% proof stress is 310 MPa and the maximum engineering stress (ultimate tensile strength) is 618 MPa. The specimen orientation did not significantly affect the stress-strain curve or the modulus.

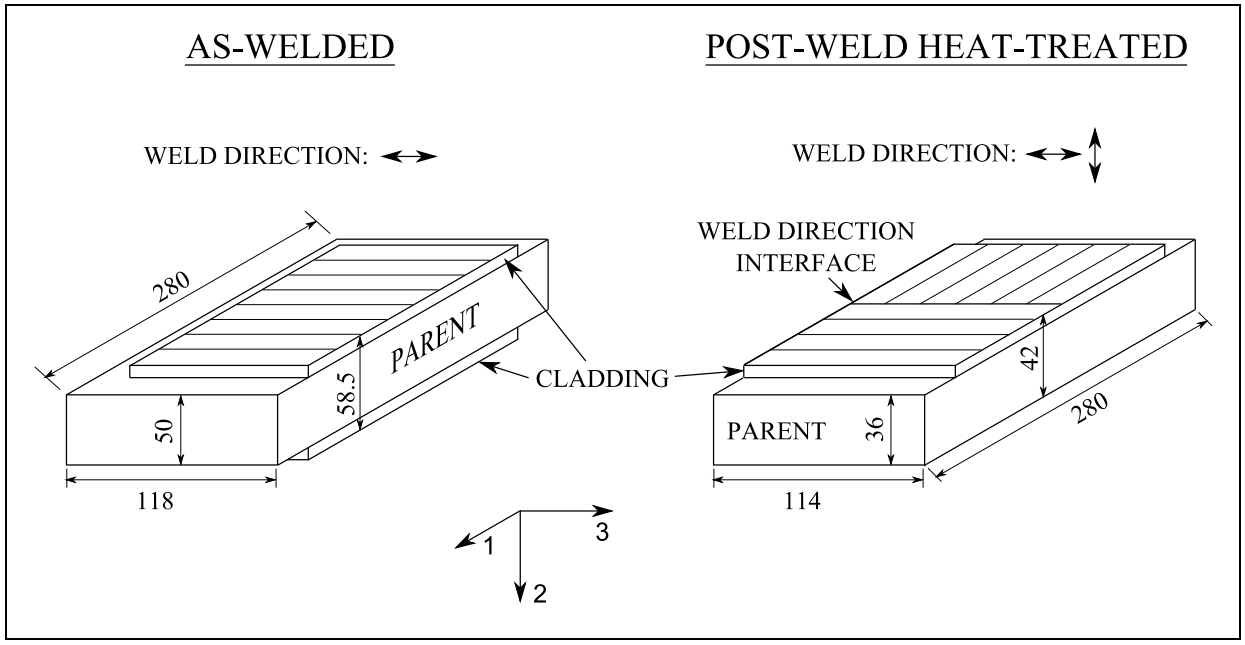

Figure 1 The two clad plates used for this work. Both are Alloy 82 cladding on SA508 Grade 4N parent. Dimensions are in mm.

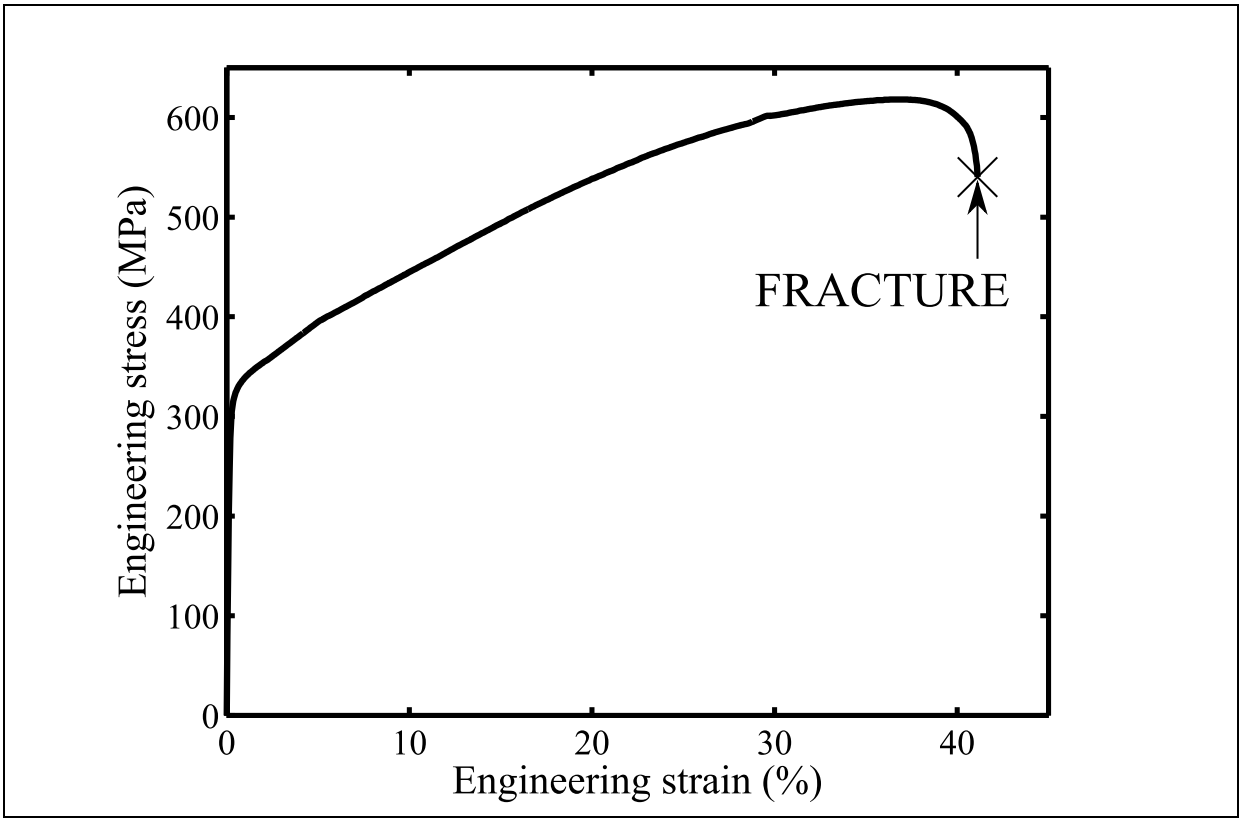

Figure 2 **Stress-strain behaviour of the Alloy 82 cladding, measured by tensile testing.**

2.3 Residual stress measurements

A range of residual stress measurement techniques were used, each with specific capabilities. Near-surface residual stress measurements were carried out using Incremental Centre Hole Drilling (ICHD) [20], which measures to a depth of half the hole diameter, usually 1 or 2 mm deep. Deep Hole Drilling (DHD) [21] was used to measure residual stresses deep inside the specimens, although accuracy is reduced within approximately 1 mm of the surface. The Contour method [22] was also used, which provides an area map of the residual stress to validate whether the line measurements obtained from DHD and ICHD are representative of the residual stresses throughout the clad plates.

The DHD measurements were carried out at the University of Bristol. Previous work by Daniel George [23] found that the DHD method may be inaccurate when measuring large stress gradients, and that the accuracy could be improved by reducing the diameter of the core which is machined as part of the measurement. A finite element study was therefore conducted as part of the work presented in this paper to investigate the accuracy of measuring large stress gradients using the DHD method with different core and reference hole diameters. It was found that the accuracy of the simulated measurement near a step change in stress improved with decreasing reference hole and core diameters. Since severe stress gradients were expected near

the interface between the cladding and parent materials, the smallest practical DHD size was employed, which uses a 1.5 mm reference hole diameter and a 5 mm trepan diameter. The ICHD measurements were carried out by Veqter Ltd to 1 mm depth (2 mm hole diameter), except ICHD5 which was 2 mm deep (4 mm hole diameter). The Contour measurement was carried out at the Open University. Several measures were taken to ensure large stress gradients or short length scale residual stresses associated with each clad layer or at the clad interface were captured including: (a) use of a small wire diameter for EDM cutting, 150 μm, to improve the quality of contour cut surfaces; (b) use of sacrificial layers on the cladding surface to prevent wire EDM cutting induced artefacts; (c) measurement of the surface contours at a fine pitch, 250 μm; (d) optimising the data processing step in order to reliably capture inherent cut surface deformations; and (e) use of an embedded cutting strategy to provide self-constraint.

These residual stress measurement techniques are all mechanical strain relaxation methods which require a value for the Young's modulus. 172.4 GPa was used for the Alloy 82, determined from tensile tests described in the previous section of this paper. 206 GPa was used for the SA508 Grade 4N steel, which is within the range of 196-207 GPa provided by Ashby and Jones for ferritic, low-alloy steel [24].

Figure 3 shows a map of measurements and operations carried out on each block. Figure 3 (a) shows the as-welded block on which a single DHD measurement was made. This measurement was performed prior to the tensile specimens being extracted, so that the cladding was intact. Figure 3 (b) shows the measurements and cuts made on the post-weld heat-treated block. The number in brackets before each measurement label indicates the order. For example, (3) ICHD3 was carried out before (4) DHD1. The block was eventually cut into three segments, labelled A, B, and C as shown in Figure 3 (b): the Contour method cut the specimen in two via a wire EDM cut, and an additional wire EDM cut was performed so that there were two segments of equal width and a third smaller segment. Only Segment A was subjected to thermal shock, which is described in more detail later in this paper.

Table 1 summarises which measurements were made before and after thermal shock on the post-weld heat-treated plate. Table 2 summarises the components of stress and region measured by each measurement method. Note that although σ_{22} has not been measured in this work, previous measurements on weld-clad pressure vessel material suggest that the components of stress normal to the cladding surface are small compared to the in-plane components [11].

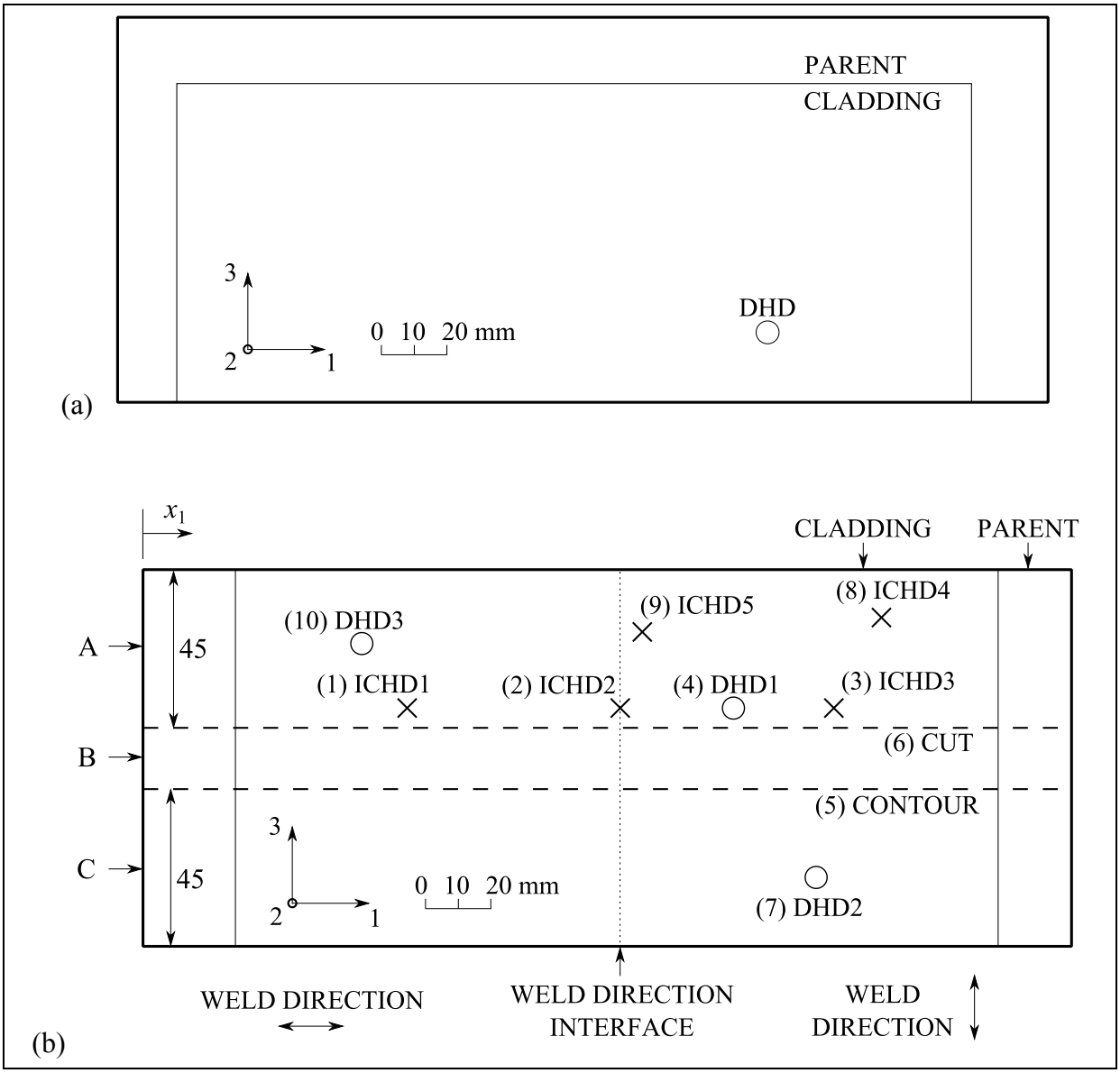

Figure 3 Position of residual stress measurements on the as-welded (a) and post-weld heat-treated (b) plates, drawn as if looking down onto the cladding surface from above. Dimensions are in mm.

Table 1 A summary of residual stress measurements carried out on the post-weld heat-treated block before and after experiencing thermal shock.

Before Thermal Shock	After Thermal Shock
ICHD1	
ICHD2	
ICHD3	ICHD4
DHD1	ICHD5
DHD2	DHD3
Contour	

Table 2 A summary of the stress components measured by each method, and the region over which stress is measured.

Method	Measured Stress Components	Measured Region
DHD	σ_{11}, σ_{33}, σ_{13}	1D line along x_2 – through-thickness.
ICHD	σ_{11}, σ_{33}, σ_{13}	1D line along x_2 – near-surface.
Contour	σ_{33}	2D area map in the x_1-x_2 plane.

2.4 Thermal shock test

The post-weld heat-treated plate was chosen for thermal shock tests since it best represents the state of the material in an RPV. Segment A in Figure 3 (b) was subjected to thermal shock using the arrangement illustrated in Figure 4. Water at a temperature of 20°C is supplied to a spray nozzle via a submersible pump. The spray nozzle is an aluminium box with 21 holes drilled on one face. The holes have a diameter of 2 mm and are arranged in two rows so that water is sprayed evenly over the specimen surface. The procedure used to subject the specimen to thermal shock was as follows. The specimen was first heated up to 480°C in a furnace. The specimen was then removed from the furnace and positioned over the spray nozzle. Finally, the nozzle pump was switched on, spraying the surface of the cladding with cold water at a rate of 13.8 l/min. The temperature throughout the specimen was monitored during heating and quenching by K-type thermocouples at three different depths which are shown in Figure 4: two were welded directly to the surface of the cladding (T1); two were secured in drilled holes at the mid-thickness (T2); and two were welded directly onto the unclad surface (T3).

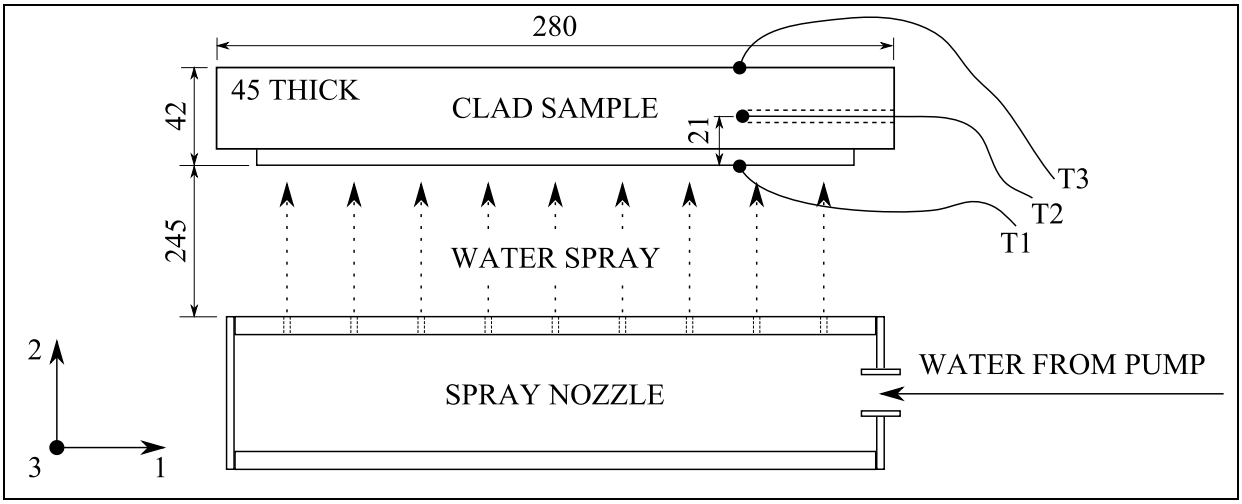

Figure 4 The arrangement used to subject the post-weld heat-treated plate to thermal shock. The thermocouples are attached at positions T1, T2, and T3. Dimensions are in mm.

3 Finite element analysis

A finite element model was made to investigate the physical causes of residual stress redistribution occurring during thermal shock. The model was analysed using the finite element code, Abaqus 6.14 [25]. The model consists of a heat transfer analysis followed by a stress analysis. The heat transfer analysis calculates the temperatures throughout the geometry at discrete increments of time during thermal shock. The results are then prescribed to the stress analysis, which calculates the stress due to thermal strain. The stress analysis also includes cladding residual stress. A schematic of the model geometry is shown in Figure 5. This is a quarter-model representation of Segment A of the heat-treated block, shown in Figure 3 (b). Symmetry boundary conditions were applied to two faces for the stress analysis. The geometry was constructed using 26,320 eight node linear brick elements of type DC3D8 for the heat transfer analysis and of type C3D8R for the stress analysis. The same geometry was used for both the heat transfer and stress analyses.

For the heat transfer analysis, the mesh was initially at a uniform temperature of 480°C. The surface of the cladding was then instantaneously adjusted to 20°C, representing thermal shock, and the transient temperature throughout the mesh was calculated at progressively larger increments of time starting with 0.02 seconds. All other surfaces were assumed adiabatic. Simulating thermal shock in this manner circumvents prescribing a film heat transfer coefficient, which is difficult to reliably calculate and in practice is not a constant value [26]. This approach is akin to prescribing an infinite film heat transfer coefficient, and so the model can be considered an upper bound or severe simulation of thermal shock. This method is satisfactory given the purpose of the model is to better-understand a physical effect rather than exactly simulate the thermal shock. Note that heat flux is non-zero in only one direction (x_2 in Figure 5), and so in theory a one-dimensional mesh could be used. A three-dimensional mesh was used instead to simplify the process of transferring the results to the stress analysis.

For the stress analysis, the mesh was initially stress-free at a temperature of 580°C, which represents a typical post-weld heat-treatment temperature. The whole model was then cooled to 20°C. The effect is to generate cladding residual stress due to the difference in thermal expansion between the cladding and parent materials. No yielding occurred during this elastic cooldown since the resulting residual stress was well below the yield strength of both materials. Finally, the transient stress during thermal shock was calculated by prescribing the time-dependent temperatures calculated in the heat transfer analysis.

Material properties used in the model are shown in Table 3 for the parent and Table 4 for the cladding. Thermal conductivity, specific heat, thermal expansion coefficient, and density were obtained from data published in the open literature [27-30]. Where data for the SA508 Grade 4N and Alloy 82 were unavailable, values for alloys with similar compositions were used instead. The thermal expansion coefficient is defined in this paper as the mean linear coefficient from 20°C to the indicated temperature, so that free linear thermal expansion is calculated by:

$$\varepsilon_{th} = \alpha(T - 20) \tag{2}$$

where ε_{th} is the thermal strain (in m/m), α is the thermal expansion coefficient (in m/m°C), and T is the current temperature (in °C). Poisson's ratio and density were assumed temperature-independent. The room temperature Young's moduli of both materials were the same as those used for residual stress measurements. The parent was assumed to be elastic perfectly plastic with a room temperature yield strength equal to the 0.2% proof stress calculated from tensile test data [31]. The Young's moduli of both materials and the yield strength of the parent were reduced at elevated temperatures using factors calculated from data published in the literature for comparable alloys [29, 32, 33]. For the elastic-plastic behaviour of the cladding, the stress-strain curve shown in Figure 2 was converted to true stress and strain, discretised, and then input into Abaqus as an incremental plasticity material with isotropic hardening. True strain, ε_t, was calculated using:

$$\varepsilon_t = \ln\left(\frac{l}{l_0}\right) \tag{3}$$

where l is the extended length and l_0 is the undeformed length. True stress, σ_t, was calculated by assuming that the specimen volume was conserved during the test:

$$\sigma_t = \frac{Fl}{A_0 l_0} \tag{4}$$

where F is the load and A_0 is the undeformed area. The yield stress shown in Table 4 is the 0.2% proof stress. The elastic-plastic behaviour of the cladding was assumed constant with temperature because tensile tests were only carried out at room temperature. In reality the yield strength of the cladding would reduce with increasing temperature [34] which could promote more residual stress redistribution than calculated by the model, although it is expected that the effect would be small because the cladding rapidly cools.

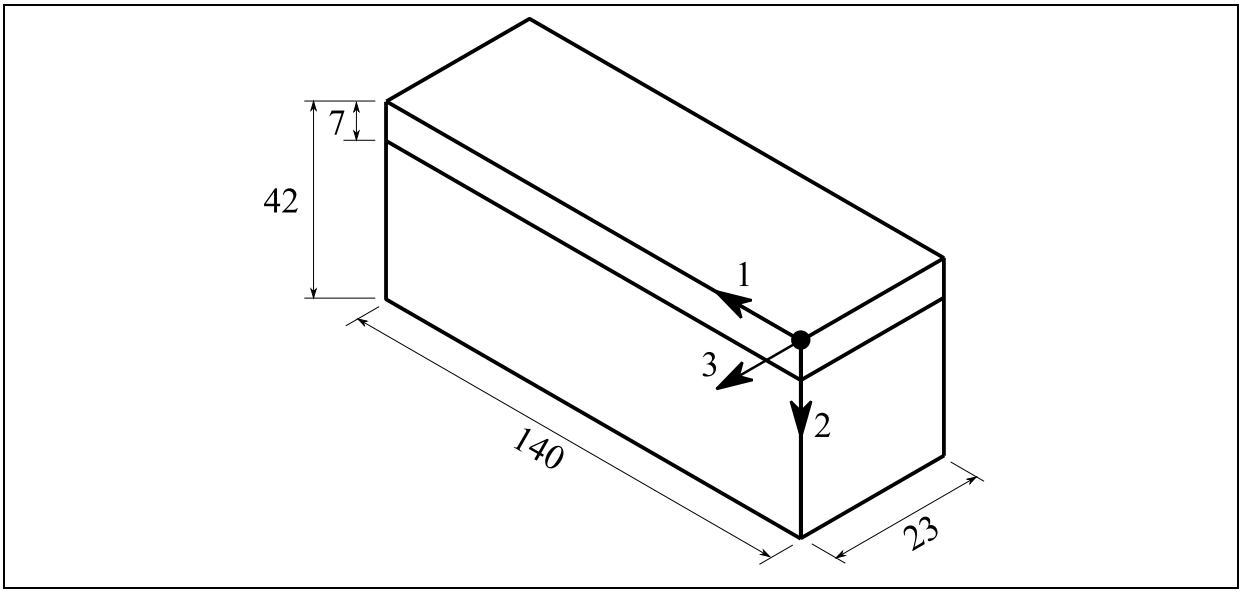

Figure 5 Geometry of the finite element model. Symmetry boundary conditions were prescribed to the $x_1 = 0$ and $x_3 = 0$ faces.

Table 3 Material properties used for the parent in the finite element analysis.

Temperature (°C)	Thermal conductivity, κ (W m^{-1} K^{-1})	Specific heat, c_p (J kg^{-1} K^{-1})	Thermal expansion coefficient, α (μm m^{-1} K^{-1})	Young's modulus, E (GPa)	Poisson's ratio, ν	Yield stress, σ_y (MPa)	Density, ρ (kg m^{-3})
20	41.6	466	11.80	206	0.3	662	7790
100	41.3	495	12.14	204	0.3	625	7790
200	40.5	532	12.29	197	0.3	599	7790
300	39.3	570	12.51	192	0.3	584	7790
400	37.2	623	13.01	183	0.3	560	7790
500	34.7	695	13.59	173	0.3	506	7790
600	31.6	795	14.04	164	0.3	393	7790

Table 4 Material properties used for the cladding in the finite element analysis.

Temperature (°C)	Thermal conductivity, κ (W m^{-1} K^{-1})	Specific heat, c_p (J kg^{-1} K^{-1})	Thermal expansion coefficient, α (μm m^{-1} K^{-1})	Young's modulus, E (GPa)	Poisson's ratio, ν	Yield stress, σ_y (MPa)	Density, ρ (kg m^{-3})
20	14.9	444	11.03	172	0.3	310	8470
100	15.9	465	11.33	169	0.3	310	8470
200	17.3	486	11.35	165	0.3	310	8470
300	19.0	502	11.35	160	0.3	310	8470
400	20.5	519	12.45	155	0.3	310	8470
500	22.1	536	14.03	151	0.3	310	8470
600	23.9	578	16.22	145	0.3	310	8470

4 Results

Note that in figures in this section, the position of the interface between the cladding and parent materials is indicated with a vertical line that is labelled 'interface'. The depth, x_2, is measured from the surface of the cladding.

4.1 Residual stress measurements in the as-welded plate

The through-thickness stress in the as-welded plate measured by DHD is shown in Figure 6. The stress is approximately symmetric, which is as expected since the as-welded block is clad on both sides. The maximum tensile stress is 650 MPa, which occurs in the parent material approximately 3 mm beneath the cladding.

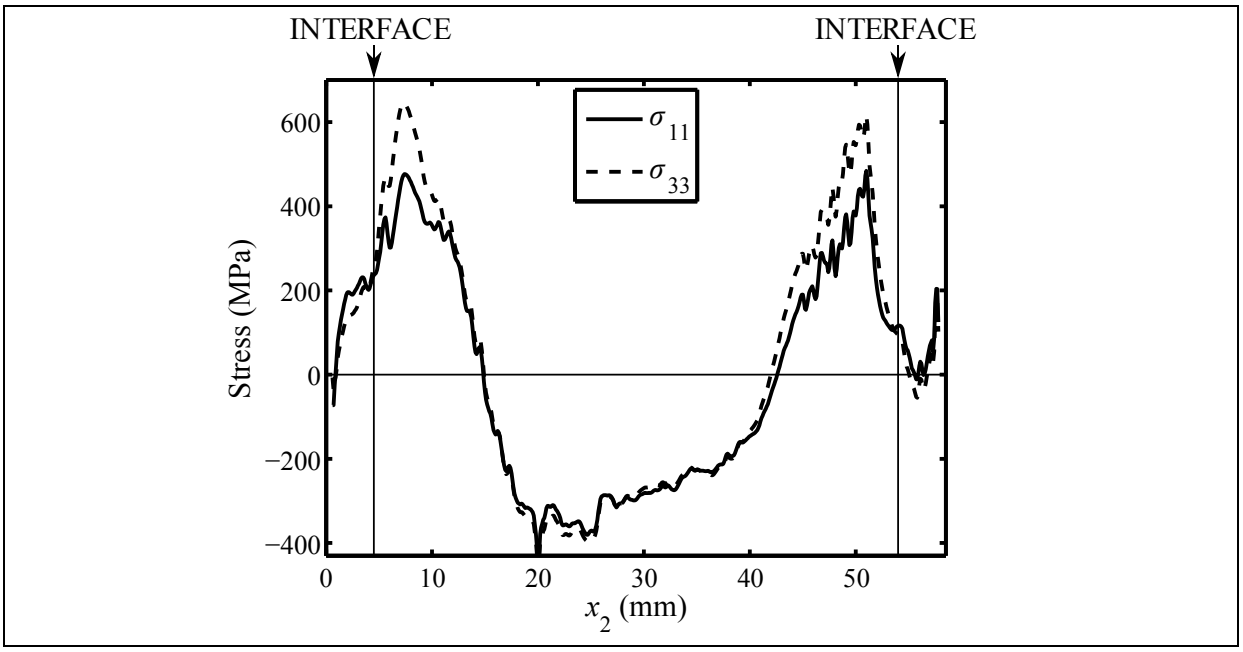

Figure 6 Residual stress in the as-welded plate measured by DHD.

4.2 Residual stress measurements in the post-weld heat-treated plate

The through-thickness residual stress of the post-weld heat-treated plate measured by DHD and a representative line of the Contour measurement is shown in Figure 7 (a) (σ_{11} component) and Figure 7 (b) (σ_{33} component). Results from the Contour measurement plotted in Figure 7 (b) were extracted at the position $x_1 = 220$ mm, where x_1 is defined in Figure 3 (b). Both the σ_{11} and σ_{33} components are tensile in the cladding and become compressive near the interface with the parent material. All measured magnitudes of stress are well below the yield strengths of the cladding (310 MPa) and the parent (662 MPa). DHD2, which was carried out after the plate was cut into three segments, shows good agreement with DHD1 and the Contour

measurement. Therefore, it can be assumed that cutting the plate caused negligible residual stress relaxation.

To investigate the variation in residual stress across the length of the plate, results from the Contour measurement were extracted at six positions: at x_1 = 50, 80, 110, 220, 225, and 230 mm, where x_1 is defined in Figure 3 (b). The mean stress calculated from the six positions is plotted in Figure 8. The error bars represent the range of values measured at the different positions. The variation of residual stress with the x_1 position is greatest at 3.5 mm beneath the cladding in the parent material, where the range of measurements is up to 86 MPa. There is less variability in the cladding (around 50 MPa) and at the back face of the specimen (around 10 MPa). The variability exists because the measurement encompasses regions with different weld directions, as shown in Figure 3 (b), and because there is some variability of residual stress with the position relative to the weld bead. The latter cause of variability has been demonstrated in previous measurements on stainless steel cladding [5].

The ICHD measurements shown in Figure 9 (a) (σ_{11} component) and Figure 9 (b) (σ_{33} component) provide a more detailed characterisation of the residual stress within 1 mm of the cladding surface. Both components of stress are compressive at the surface. The magnitude and shape of the stress is strongly dependent on direction: the σ_{11} component of stress changes sign between 0.5 and 0.8 mm deep, and the σ_{33} component changes sign between 0.1 and 0.2 mm.

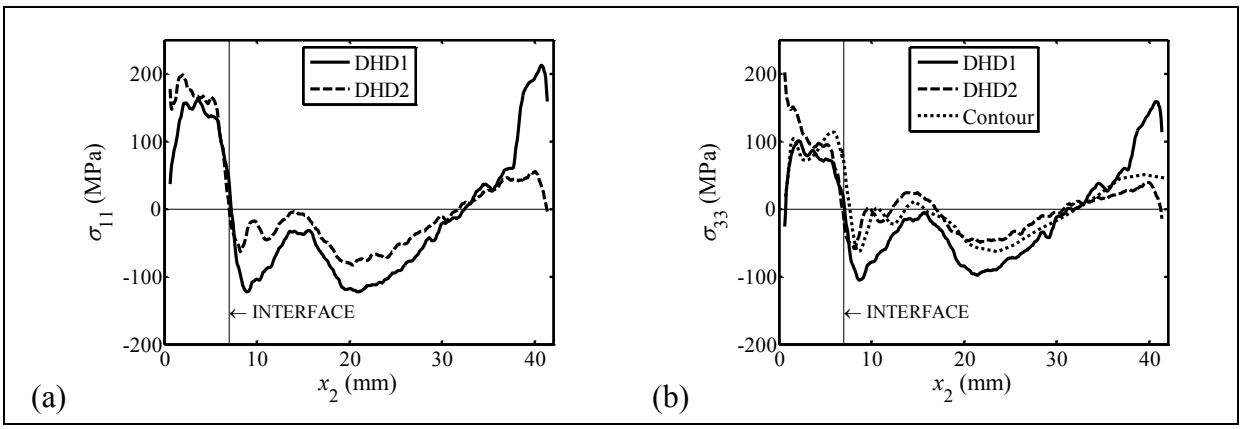

Figure 7 Through thickness residual stress in the post-weld heat-treated plate measured using DHD and Contour methods. The σ_{11} component is shown in (a), and the σ_{33} component in (b).

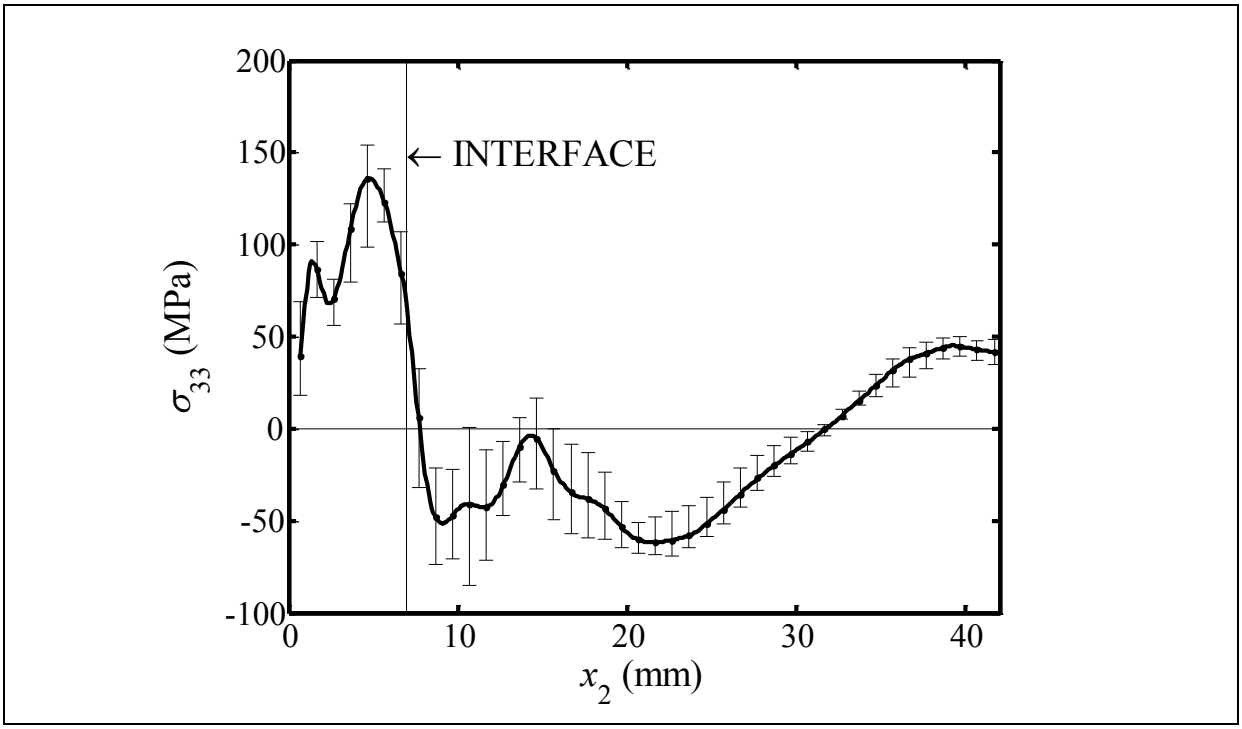

Figure 8 The range of through-thickness residual stresses measured by the Contour method at different positions across the post-weld heat-treated plate.

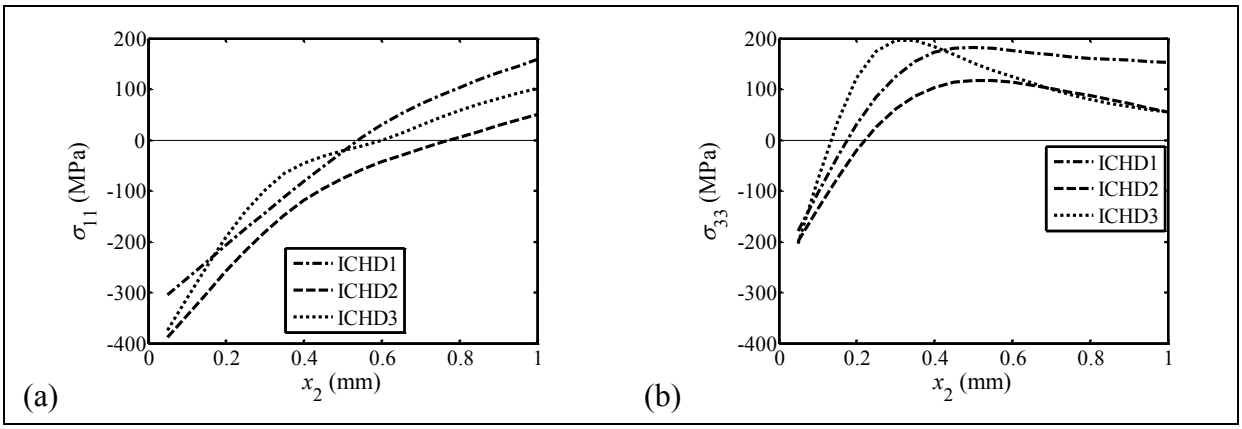

Figure 9 Near-surface residual stress in the post-weld heat-treated plate measured by ICHD. The σ_{11} component is shown in (a), and the σ_{33} component in (b).

4.3 Rate of cooling during thermal shock

The temperatures measured in the post-weld heat-treated plate during thermal shock are shown alongside the temperatures in the finite element model in Figure 10. In the experiment, the surface of the cladding cooled by 370°C within the first second of thermal shock. In the model, the surface of the cladding was instantaneously adjusted to 20°C as a prescribed boundary condition. Cooling at the back face was slower in the model than the experiment. This is

because in the model heat transfer only occurred from the cladding surface, and all other surfaces were assumed adiabatic. In the experiment, heat transfer occurred from these surfaces by radiation, free convection from air cooling, and by unintended splashing from the water spray.

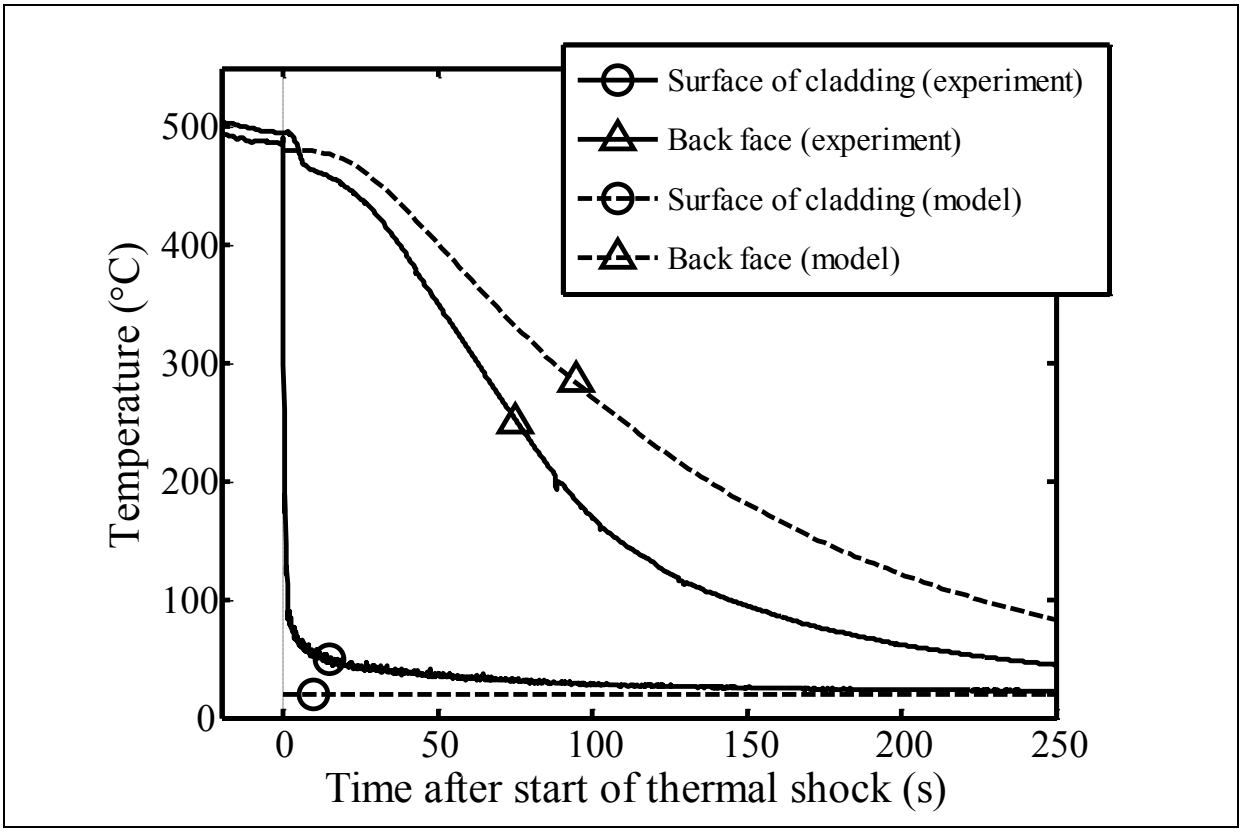

Figure 10 Temperatures in the post-weld heat-treated plate during thermal shock.

4.4 Residual stress measurements after thermal shock

Figure 11 compares DHD measurements made on the post-weld heat-treated plate before and after it was subjected to thermal shock. The σ_{11} component of stress is shown in Figure 11 (a) and the σ_{33} component in Figure 11 (b). The before thermal shock curve is the average of DHD1 and DHD2, with the error bars indicating the range of values from the two measurements. The after thermal shock curve is the result of DHD3. Whereas before thermal shock the residual stress is tensile throughout the cladding, after thermal shock both components of stress are compressive to a depth of 2.6 mm. Residual stress redistribution occurred to a depth of approximately 10 mm for the σ_{33} component, and deeper for the σ_{11} component.

The near-surface residual stresses measured by ICHD on the post-weld heat-treated plate before and after thermal shock are shown in Figure 12. The σ_{11} component of stress is shown in Figure 12 (a) and the σ_{33} component in Figure 12 (b). The before thermal shock curve is the average result of ICHD1, ICHD2, and ICHD3. The after thermal shock curve is the average result of ICHD4 and ICHD5. The error bars indicate the range of values obtained by the

different measurements. Whereas before thermal shock the near-surface residual stress is strongly direction-dependent, after thermal shock the stress is approximately equi-biaxial. The residual stress after thermal shock is also entirely compressive throughout the measurement depth, which shows good agreement with the DHD measurements shown in Figure 11.

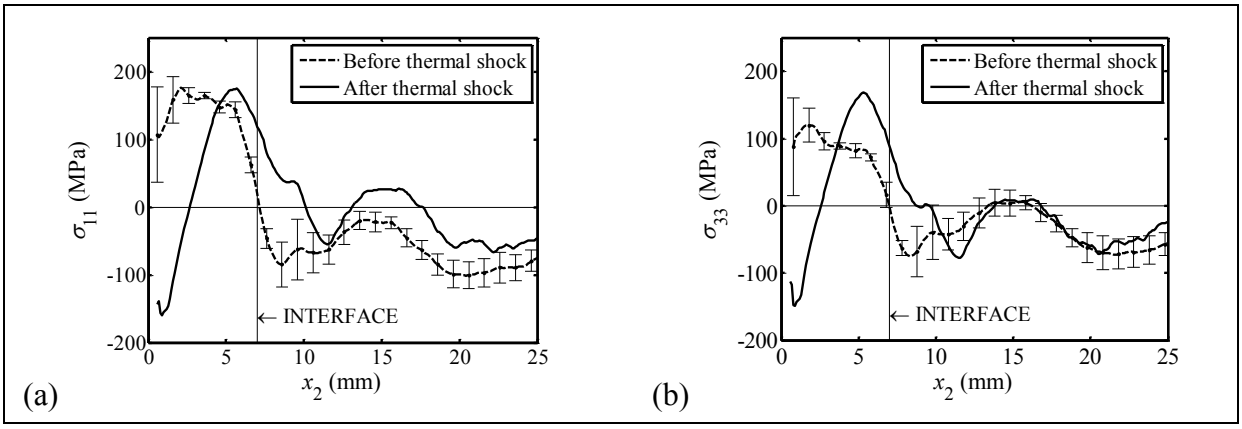

Figure 11 Comparison of DHD measurements on the post-weld heat-treated plate before and after thermal shock. The σ_{11} component is shown in (a), and the σ_{33} component in (b). Error bars indicate the range of values measured by DHD1 and DHD2 before thermal shock.

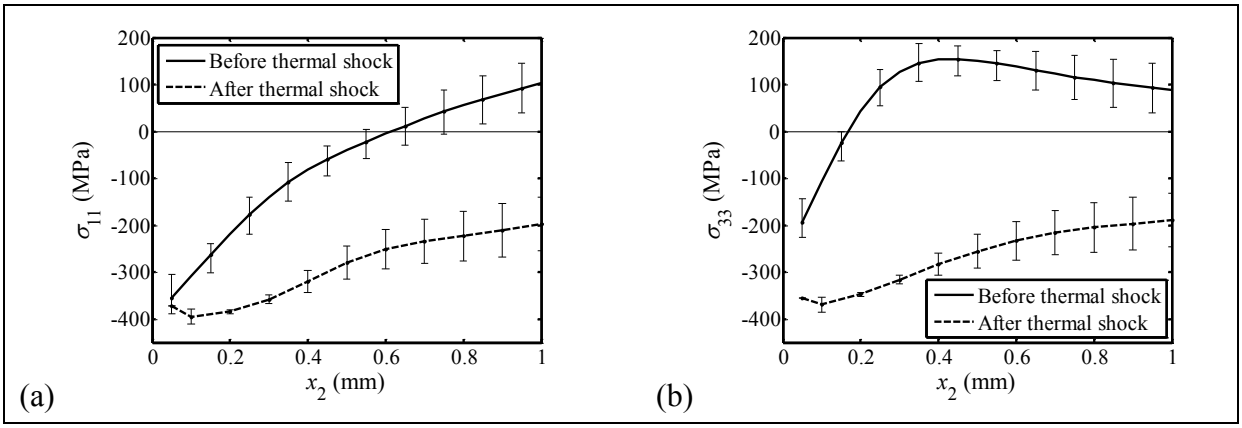

Figure 12 Near-surface residual stress before and after thermal shock measured by ICHD. The σ_{11} component is shown in (a), and the σ_{33} component in (b). Error bars indicate the range of values obtained from different measurements.

4.5 Finite element analysis

Figure 13 shows the residual stress at 20°C calculated by the finite element model before and after thermal shock. Before thermal shock the residual stress arises due to the difference in thermal expansion between the cladding and parent materials on cooling from zero stress at 580°C. The stress in each material is a combination of uniaxial stress and bending. The shape and magnitude of the predicted residual stress does not perfectly match the measurements, for example shown in Figure 7 (a), but the prediction is broadly representative: i.e. the residual stress is tensile in the cladding, compressive beneath the cladding in the parent, and tensile at the back face. After thermal shock the finite element model predicts yield-magnitude

compressive stress at the surface of the cladding and smaller tensile stress towards the interface. The bending component of stress in the parent has changed direction and the stress directly beneath the interface is now tensile. The material in the parent does not yield during the simulation, and so the redistribution in the parent is entirely due to yielding in the cladding.

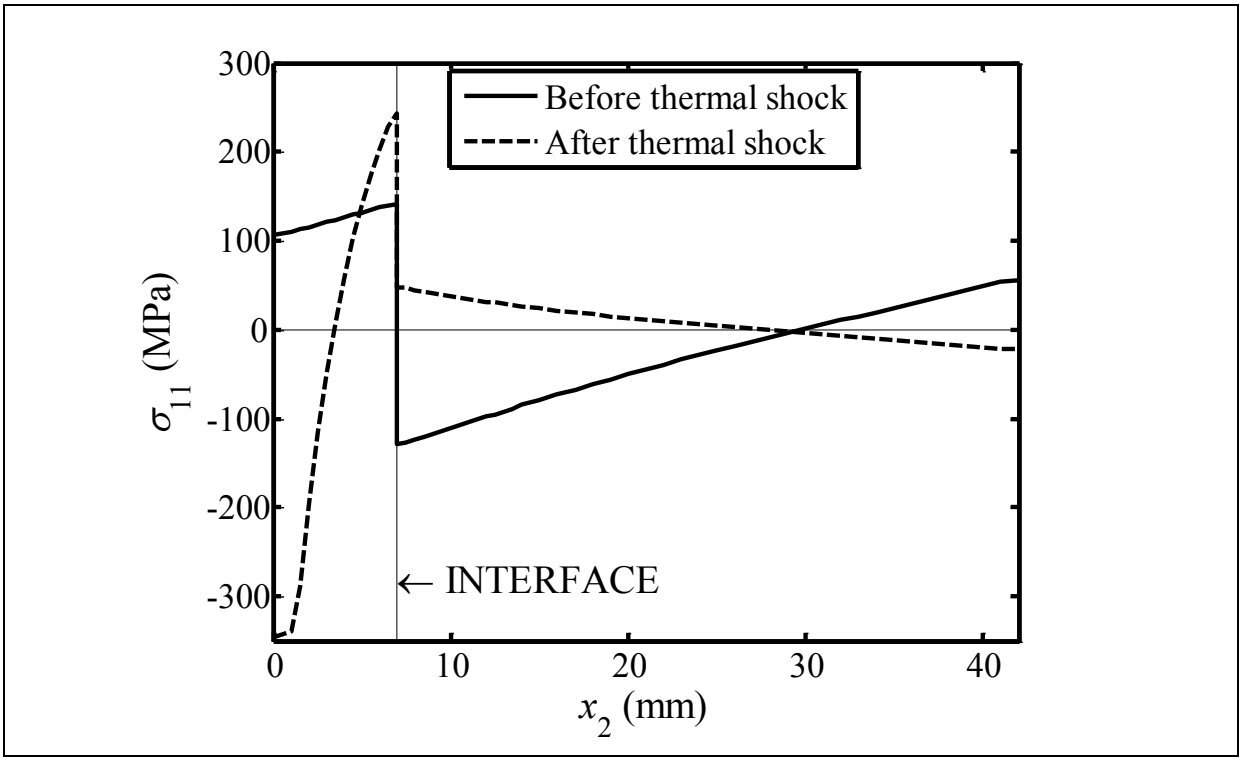

Figure 13 Residual stress calculated before and after thermal shock using finite element analysis.

5 Discussion

5.1 Residual stress in as-welded and post-weld heat-treated material

The residual stresses through the whole thickness of the as-welded and post-weld heat-treated plates are shown in Figure 6 (as-welded), and Figure 7 and Figure 8 (post-weld heat-treated). The residual stresses in both plates are compared in Figure 14 just near the cladding. The depth from the cladding surface, x_2, has been normalised by the thickness of the cladding, t_c, because the cladding thickness is different in each plate. Residual stress is plotted down to a depth of only three times the cladding thickness, so that the difference in stress is mainly due to differences in heat-treatment rather than geometry. The as-welded result is from the single DHD measurement carried out on the as-welded plate. The post-weld heat treated result is the average of DHD1 and DHD2, and the error bars indicate the range of values from the two measurements. The stress in the cladding is mostly tensile and of similar magnitude in both as-

welded and heat-treated conditions. Directly beneath the cladding, the heat-treated block contains low-magnitude compressive stress whereas the as-welded block contains high-magnitude tensile stress with a peak of around 480 MPa. Similar findings have been reported in previous work on stainless steel cladding, where the main benefit of performing post-weld heat-treatment has been to reduce tensile stresses in the parent without causing significant redistribution in the cladding [2-4, 11]. The benefits to structural integrity of carrying out post-weld heat-treatment are quantified using stress intensity factor calculations later in this paper.

The through-thickness residual stress measured in the post-weld heat-treated material, for example shown in Figure 7 and Figure 8, is similar both in terms of magnitude and shape to measurements reported by Jones et al [6] on similar-sized post-weld heat-treated plates (38 mm total thickness) clad with 6 mm of either 308/309 stainless steel or Alloy 600 nickel-based alloy. Most measurements on clad pressure vessel steel presented in the literature are through-thickness measurements and so the compressive near-surface stresses, for example shown in Figure 9, are not commonly reported. However, similar compressive surface stresses have been previously measured in milled and polished 309/316 stainless steel cladding using ICHD and X-ray diffraction [35].

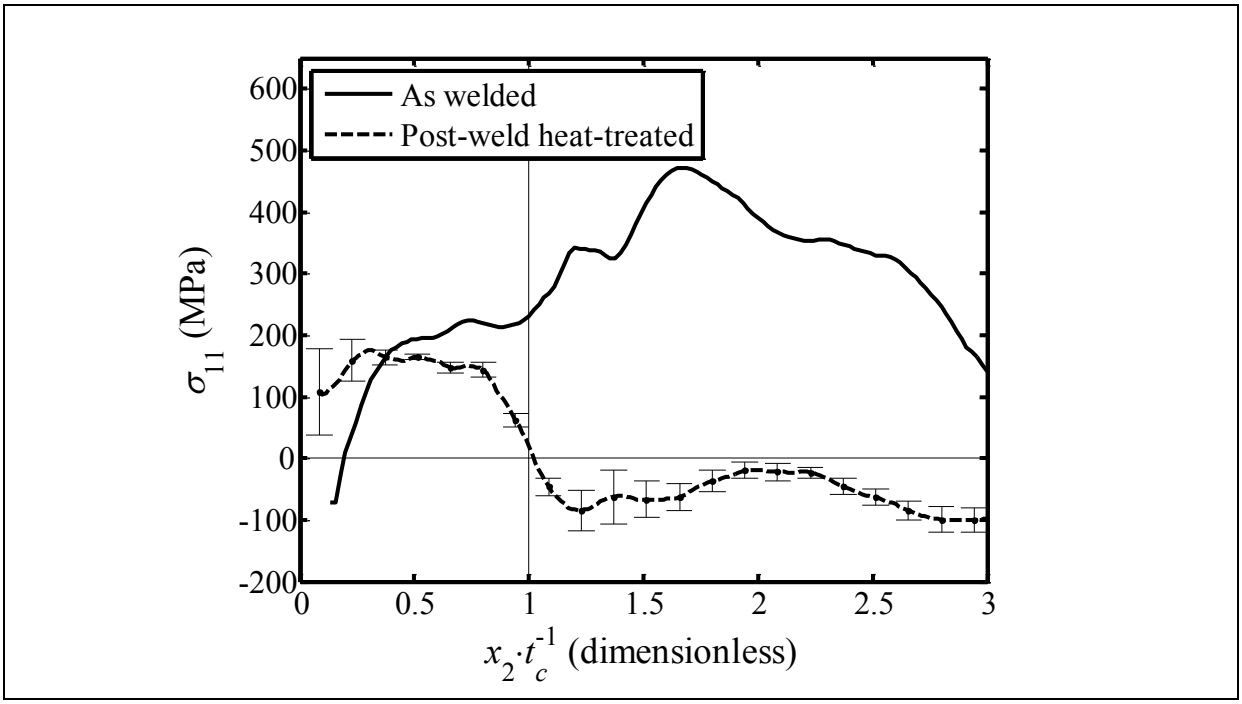

Figure 14 A comparison of residual stresses in the as-welded and post-weld heat-treated plates, plotted to a depth of three times the cladding thickness (t_c).

5.2 The effect of thickness on cladding residual stress

Residual stress measurements presented in this paper were carried out on 42 mm (post-weld heat-treated) and 58 mm (as-welded) thick plates, whereas RPVs have much thicker walls, typically around 180 – 200 mm. Measurements in previous work by James et al [9] showed that the residual stress in a clad plate was significantly affected by reducing the thickness of the plate from 80 mm to 30 mm. Rybicki et al [36] extracted 32 mm thick samples from a larger clad plate, and found that reducing the thickness of the cladding by half from 8.9 to 4.4 mm significantly increased the magnitude of residual stress in the cladding. The results from this latter study suggested that the relative thickness of the cladding and parent materials had a significant effect on the residual stress in post-weld heat-treated material. Therefore, a finite element investigation is presented here to estimate the effect of plate thickness on the magnitude of cladding residual stress in post-weld heat treated material, so that the measurements made in this work could be scaled up to a full-size RPV. The model geometry is shown in Figure 15. This is a plane stress model constructed and analysed using 8-node quadrilateral elements of type CPS8R in Abaqus 6.14 [25]. The model was initially stress-free, and then the temperature was uniformly reduced by ΔT. This is the same method of generating residual stress used in the thermal shock model described in Section 3: i.e. it is assumed that all of the cladding residual stress arises because of the difference in thermal expansion between the cladding and parent on cooling from a state of zero stress during post-weld heat-treatment. The thickness of the parent was then reduced in steps by deleting elements, and the retained residual stress was calculated at each step. The cladding and parent materials were both linear-elastic with a Poisson's ratio of 0.3, and a Young's modulus of 206 GPa in the parent and 172.4 GPa in the cladding.

Figure 16 shows how the residual stress in the cladding varies with the thickness of the parent. On the y-axis, the average residual stress in the cladding, σ_{av}, is normalised by the Young's modulus of the cladding, E_c, the difference in thermal expansion coefficient between the two materials, $\Delta\alpha$, and the change in temperature used to generate residual stress, ΔT. On the x-axis, the thickness of the parent, t_p, is normalised by the thickness of the cladding, t_c. The geometries of the post-weld heat-treated plate used in this work and a typical RPV are located on the x-axis in Figure 16. The plate has a nominal cladding thickness of 6 mm and a parent thickness of 36 mm. The typical RPV was assumed to have a cladding thickness of 6 mm and a parent thickness of 180 mm. The corresponding values on the y-axis are 0.59 for the plate and 0.9 for the RPV. Therefore, the magnitude of cladding residual stress is 1.5 times greater in the typical RPV than in the plate. Whilst the residual stress in this model was generated simply by cooling from a stress-free temperature rather than a full simulation of welding followed by heat-treatment, this basic method has been shown in this work (Section 4.5) and in previous work [36] to provide a reasonable estimate of the cladding residual stresses after post-weld heat-treatment. Therefore, the residual stress in a full-thickness RPV could be estimated by multiplying the residual stresses measured on the post-weld heat-treated plate in this work (before it was subjected to thermal shock) by a factor of 1.5. Referring to Figure 7

(a), this would increase the magnitude of residual stress in the cladding from 150-200 MPa to 225-300 MPa which is close to the yield strength of the Alloy 82 (310 MPa).

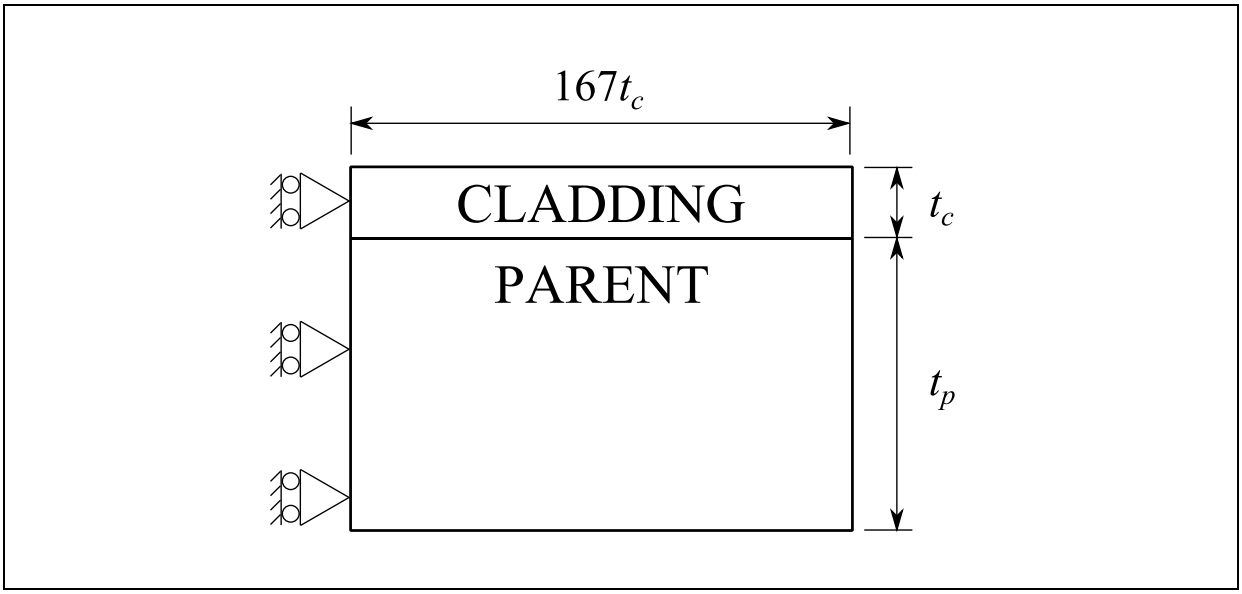

Figure 15 Geometry of the finite element model used to investigate the effect of plate thickness on the magnitude of cladding residual stress.

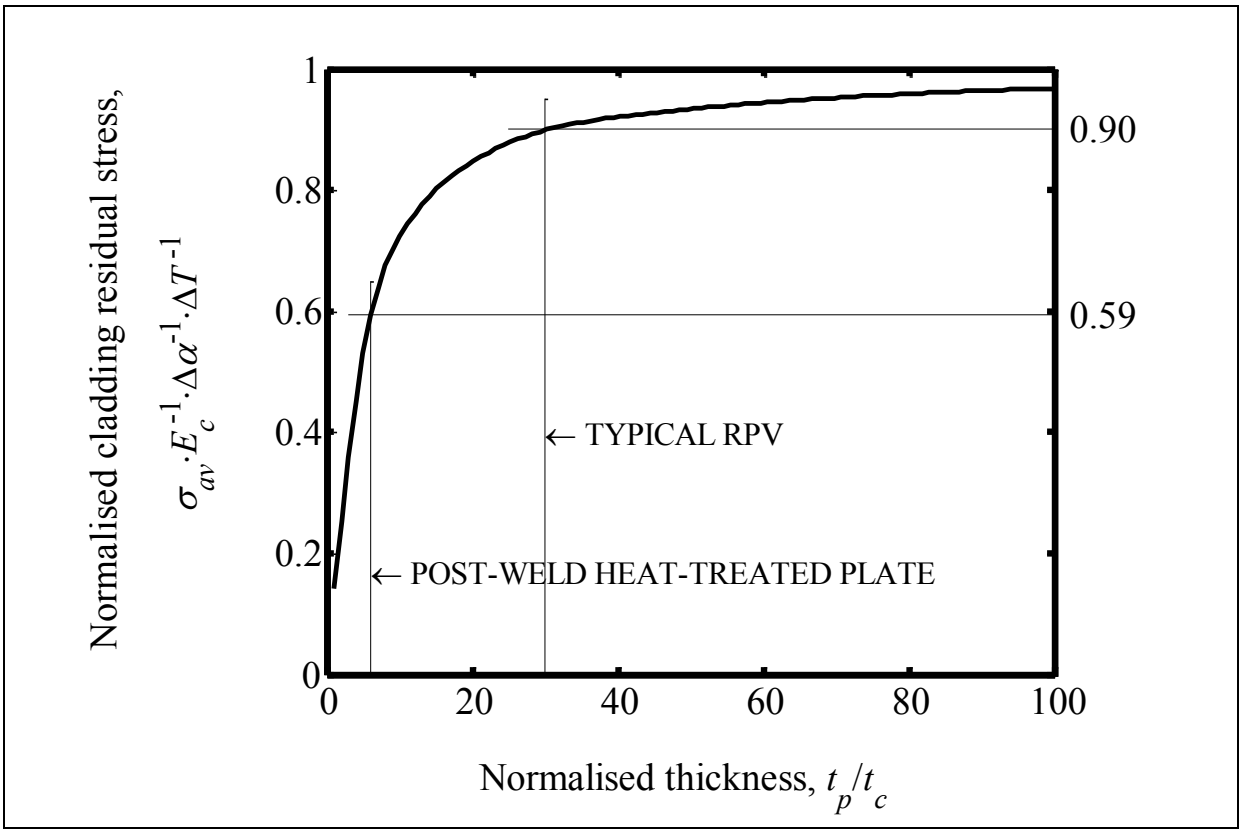

Figure 16 The average residual stress in the cladding (σ_{av}) for different ratios of parent to cladding thickness.

5.3 Stress intensity factors due to residual stress

One motivation behind characterising residual stress in RPVs is so that the contribution of residual stress to failure by fracture can be accounted for. Therefore, a basic cracked-body analysis has been carried out using the weight function method to calculate the stress intensity factor resulting solely from residual stress loading, K_{RS}. The geometry of the model is shown in Figure 17. This is a two-dimensional model of a semi-infinite plane with a one-dimensional through crack of length a extending from the edge. This configuration represents a surface defect, which in practice could arise by stress corrosion cracking. The following calculation for an edge crack in a semi-infinite plane presented by Wu and Carlsson [37] was used:

$$K_{RS} = \sqrt{a} \int_0^1 \sigma_{11}(X_2) \cdot m(X_2) \cdot dX_2 \tag{5}$$

$$m(X_2) = \frac{1}{\sqrt{2\pi}} \cdot \sum_{i=1}^{5} \beta_i (1 - X_2)^{i-\frac{3}{2}} \tag{6}$$

In Equation (5), σ_{11} is the stress normal to the crack, X_2 is x_2/a, and m is the weight function. In Equation (6), β_i is a set of coefficients. Equation (5) was evaluated using trapezoidal numerical integration. The inputs σ_{11} and X_2 were refined near the crack tip using linear interpolation so that the integral in Equation (5) could be accurately evaluated near the singularity of the weight function at $X_2 = 1$. Note that the weight function used here was for a semi-infinite rather than finite-width plate so that the stress intensity factor for a given crack length depends only on the measured residual stress, and not the thickness of the plate.

Figure 18 compares the stress intensity factors calculated using the residual stresses measured in the post-weld heat-treated and as-welded plates. Results for the heat-treated plate are presented both before thermal shock (BTS) and after thermal shock (ATS). The crack length, a, has been normalised by the thickness of the cladding, t_c, because the cladding thickness is different in each plate. For the as-welded material, the input stress in Equation (5), σ_{11}, was set to the results of the single DHD measurement carried out on the plate. For the post-weld heat-treated plate before thermal shock, σ_{11} was the average of ICHD1, 2, and 3 up to 1 mm deep, and the average of DHD1 and DHD2 thereafter. For the calculation after thermal shock, σ_{11} was set to the average of ICHD4 and ICHD5 up to 1 mm deep, and DHD3 thereafter.

The benefit of subjecting the material to a post-weld heat-treatment can be demonstrated by comparing the as-welded curve with the post-weld heat-treated BTS curve. The stress intensity factor is much higher in the as-welded plate than in the heat-treated plate, except for cracks shorter than the cladding thickness for which the magnitudes are similar in both as-welded and

heat-treated conditions. The maximum value of K_{RS} is 3.4 times greater in the as-welded condition than in the post-weld heat-treated condition.

Now comparing results for the post-weld heat-treated plate before and after thermal shock, K_{RS} was reduced after thermal shock for surface cracks shorter than the cladding thickness. The difference in K_{RS} is small for deeper defects. This is an important result since it allows better judgement of the structural integrity of an RPV that is expected to re-enter service after experiencing thermal shock due to a fault.

Note that the plate thickness effect discussed in the previous section would also mean that K_{RS} could be significantly different in a full-thickness RPV than in the relatively thin plates measured in this work. For example, the analysis in the previous section estimated that the magnitude of residual stress in a 180 mm thick RPV would be 1.5 times larger than in the 42 mm thick post-weld heat-treated plate. Therefore, the stress intensity factors calculated by Equation (5) would also be 1.5 times greater than shown in Figure 18 for the post-weld heat-treated plate before thermal shock. The maximum K_{RS} for a surface crack in an RPV would then be 28 MPa $m^{1/2}$, for a 6 mm crack.

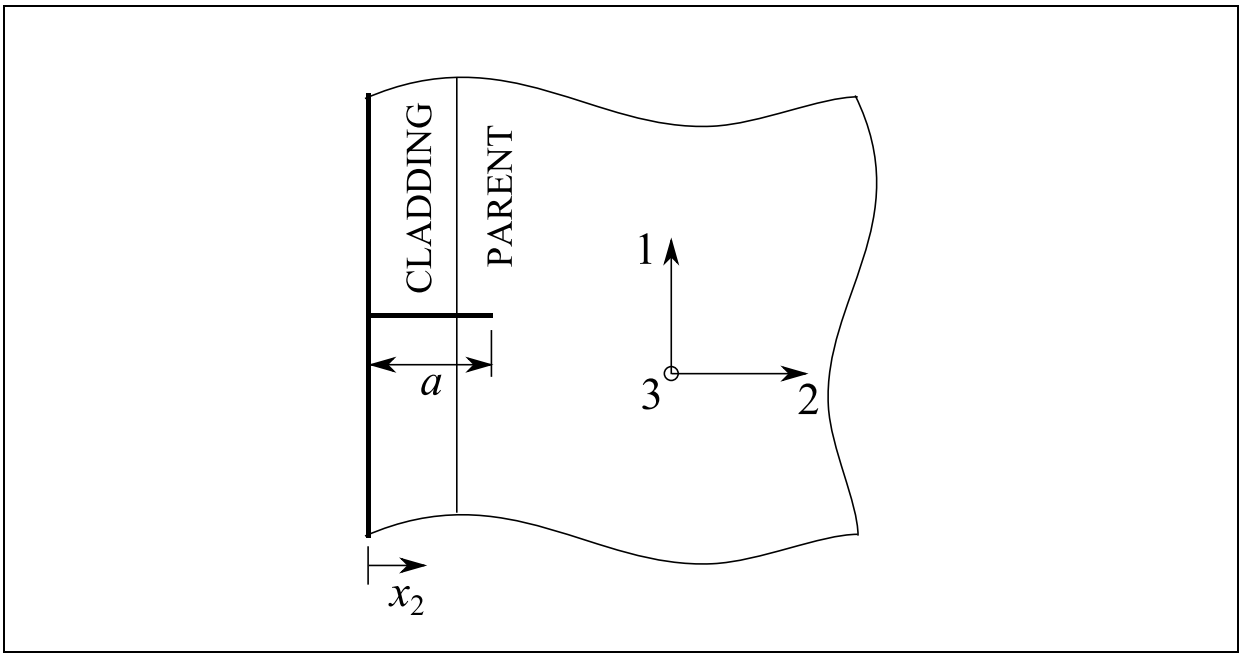

Figure 17 The geometry used for calculation of stress intensity factors induced by the measured residual stress distributions: a semi-infinite plane with a through-crack on one edge.

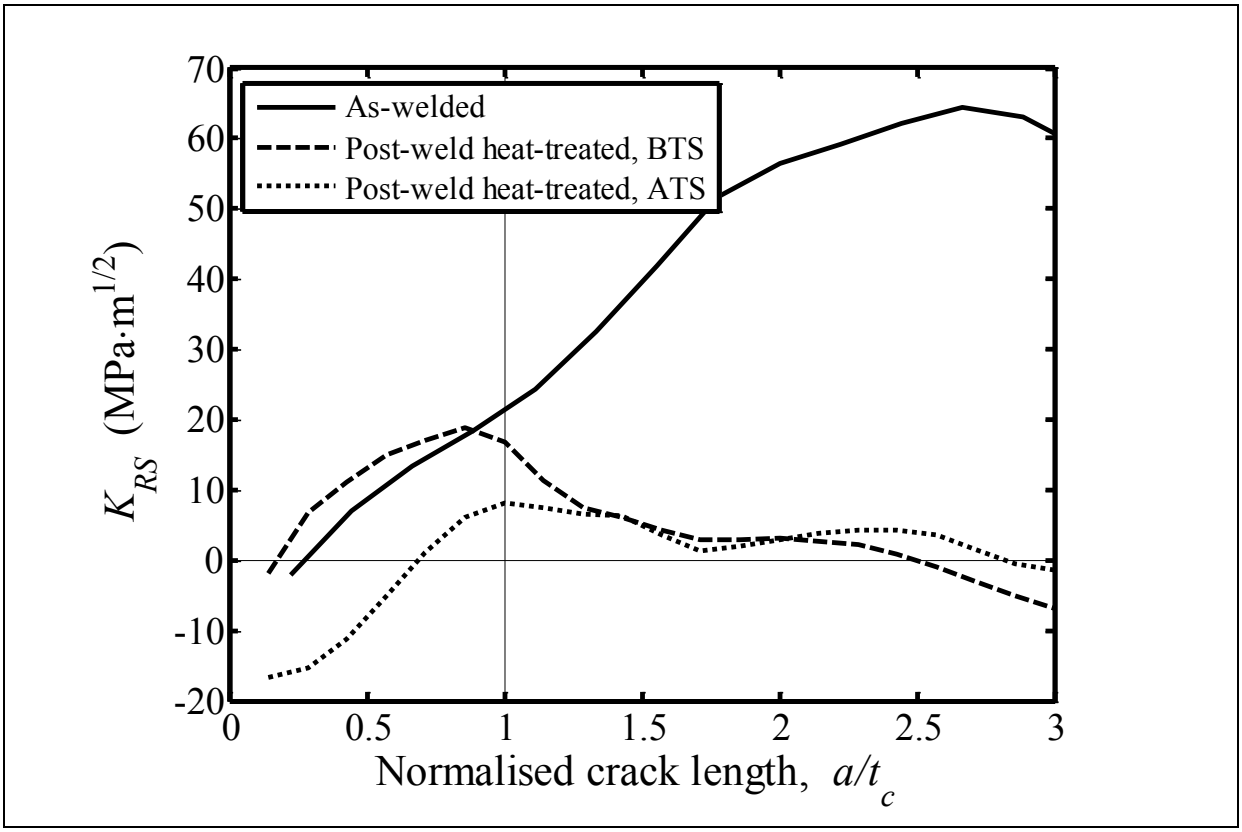

Figure 18 Stress intensity factors due to residual stress in the as-welded plate, and in the post-weld heat-treated plate before thermal shock (BTS) and after thermal shock (ATS).

5.4 General discussion

In the simple finite element model presented in Section 3 the parent material was assumed elastic perfectly plastic and the yield stress of the cladding was assumed temperature-independent (see Table 4) because only limited data was available for these materials. The first assumption is inconsequential because the parent material did not yield during the simulation. Trials were conducted to assess the validity of the second assumption and it was found that using a temperature-dependent yield stress for the cladding made only a small difference. For example, the finite element model was re-run with the yield stress of the cladding reduced by 26% at 600°C compared with the value at 20°C (the reduced value at 600°C was estimated using data given in reference [34]). Compared with the results shown in Figure 13, which were calculated using room-temperature values for yield stress at all temperatures, the residual stress after thermal shock was only different by a small amount: the maximum error at any depth (x_2) was 36 MPa. The residual stress before thermal shock was unchanged because no yielding occurred during this step in the model. Therefore, using the room-temperature stress strain curve for the cladding at all temperatures was considered satisfactory for this work.

It was shown in Figure 11 that subjecting the post-weld heat-treated plate to thermal shock caused significant residual stress redistribution to a depth of at least 10 mm beneath the surface of the cladding. The residual stress after thermal shock simulated using FEA and measured using DHD3 and ICHD5 is shown in Figure 19. The measurements in the cladding broadly match the finite element prediction: the stress is compressive near the surface and tensile near the interface. This is similar to the shape of near-surface stresses measured in previous work on quenched bars [38], and in quenched cylinders and spheres [39]. The finite element model predicted significant residual stress redistribution throughout the parent (see Figure 13), which was caused by yielding and redistribution in the cladding since no yielding occurred in the parent. Given that the thermal shock simulated by the finite element model was impractically severe, it is reasonable to suggest that the measured redistribution in the parent material, although shallower and less significant than in the model, occurred by the same mechanism.

One of the objectives of this work was to experimentally demonstrate that residual and thermal stresses interact in an inelastic manner during thermal shock when their elastically-combined magnitudes exceed yield. This has been achieved by measuring significant residual stress redistribution after thermal shock. It has been demonstrated in previous work that residual stress relaxation can occur when combined with mechanical load [16, 17], whereas this work has demonstrated redistribution solely due to thermal load. Therefore, to combine the thermal and residual stresses elastically, for example using Equation (1) from the R6 structural integrity assessment procedure, could be conservative for some defects. For example, for surface defects shorter than the cladding thickness, Figure 18 shows that K_{RS} has reduced by up to 22 MPa $m^{1/2}$. It would be interesting to investigate in future work whether K_{tot} in Equation (1) could be more accurately calculated by using the final (i.e. after thermal shock) value of K_{RS} rather than the initial value obtained from the post-weld heat-treated cladding residual stress (i.e. before thermal shock).

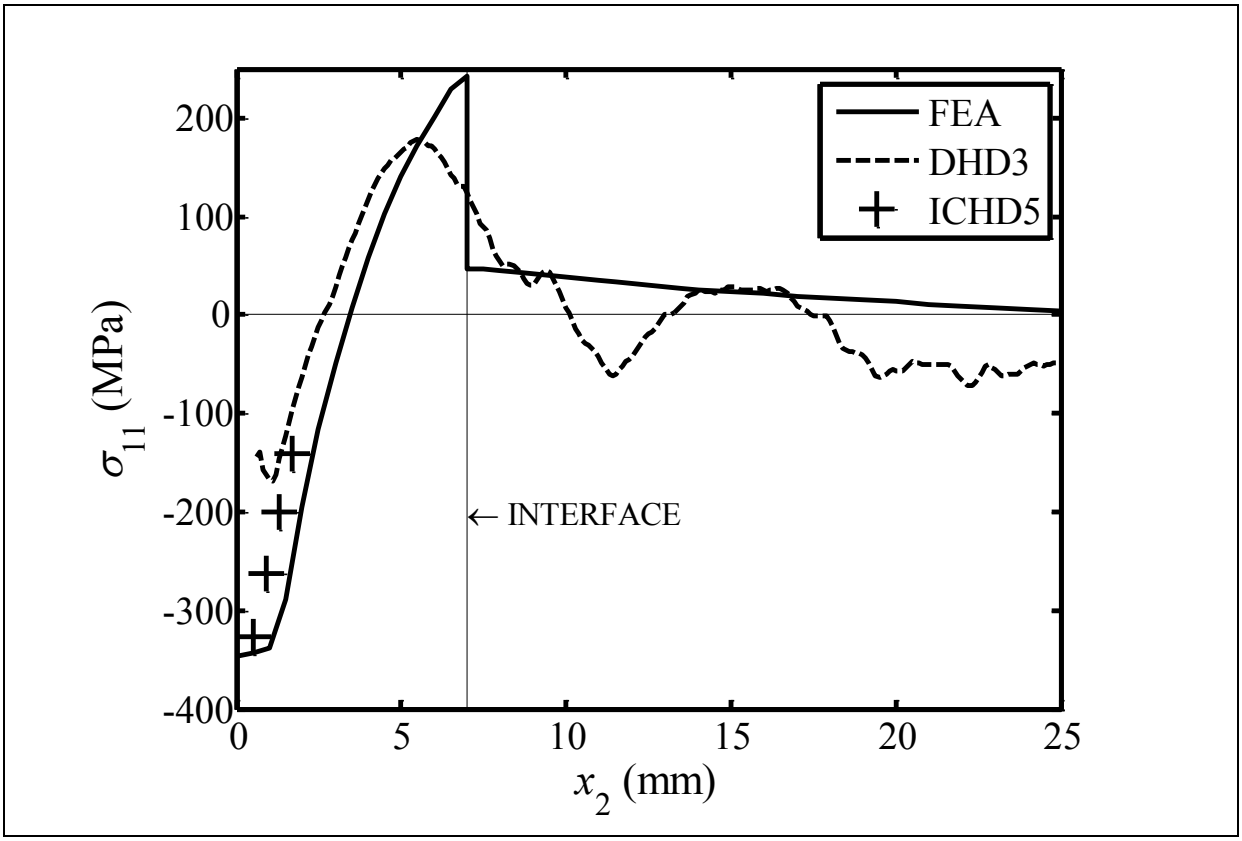

Figure 19 Residual stress in the post-weld heat-treated block after being subjected to thermal shock, simulated using FEA and measured using DHD3 and ICHD5.

6 Conclusions

This work measured the residual stress in two plates of SA508 Grade 4N nuclear pressure vessel steel, clad with Alloy 82 nickel-based alloy. One plate was as-welded, the other post-weld heat-treated. The post-weld heat-treated plate was subjected to thermal shock, and the residual stress was measured again afterwards. A finite element simulation was made to investigate the physical mechanisms causing residual stress redistribution during thermal shock.

Residual stress was mostly tensile in the cladding in both the as-welded and post-weld heat-treated material, except within 0.5 mm of the surface of the cladding where the stress was compressive. Post-weld heat-treatment caused significant residual stress relaxation in the parent, but only moderate residual stress redistribution in the cladding.

It was demonstrated that the relative thickness of the cladding and parent materials significantly affects the magnitude of cladding residual stress. Hence, the magnitude of residual stress would be greater in a full-thickness RPV than in smaller mock-ups such as those measured in this work. From the measurements made in this work, it was estimated that the residual stress in the cladding of a full-thickness post-weld heat-treated RPV would be 225-310 MPa. The peak stress intensity factor due to residual stress would be 28 MPa $m^{1/2}$ for a surface defect.

Subjecting the post-weld heat-treated material to thermal shock caused significant residual stress redistribution to a depth of at least 10 mm from the surface of the cladding. This demonstrates that the thermal and residual stresses interacted in an inelastic manner, and that combining them elastically, as suggested in the R6 structural integrity assessment procedure, could be conservative for some defects. The stress intensity factor for surface cracks shorter than the cladding was up to 22 MPa $m^{1/2}$ lower after thermal shock, whereas deeper cracks were not significantly affected.

7 Acknowledgements

The authors are grateful to Wood and the Engineering and Physical Science Research Council for funding this work. Peter James and John Sharples at Wood provided valuable advice and input. VEQTER Ltd carried out the ICHD measurements used in this paper, and Rolls-Royce supplied the clad plates. William Brayshaw at the University of Manchester provided unpublished tensile test data on the SA508 Grade 4N steel.

8 References

[1] A.M. Clayton, Thermal shock in nuclear reactors, Prog. Nucl. Eng. 12 (1) (1983) 57-83. https://doi.org/10.1016/0149-1970(83)90025-2

[2] P. Dupas, D. Moinereau, Evaluation of cladding residual stresses in clad blocks by measurements and numerical simulations, J. Phys. IV 6 (C1) (1996) 187-196. https://doi.org/10.1051/jp4:1996118

[3] H.A. Schimmoeller, J.L. Ruge, Estimation of residual stresses in reactor pressure vessel steel specimens clad by stainless steel strip electrodes, in: Residual stresses in welded construction and their effects – Volume 1, The Welding Institute, Cambridge, 1978, pp. 251-258.

[4] J. Katsuyama, H. Nishikawa, M. Udagawa, M. Nakamura, K. Onizawa, Assessment of residual stress due to overlay-welded cladding and structural integrity of a reactor pressure vessel, J Press. Vessel Technol. 135 (5) (2013) p. 051402. https://doi.org/10.1115/1.4024617

[5] R. Kume, H. Okabayashi, T. Naiki, Internal stresses in thick plates weld-overlaid with austenitic stainless steel (Report 1), Trans. Jpn. Weld. Soc. 5 (1) (1974) 32-38.

[6] D. P. Jones, W. R. Mabe, J. R. Shadley, E. F. Rybicki, Residual stresses in weld-deposited clad pressure vessels and nozzles, J Press. Vessel Technol. 121 (4) (1999) 423-429. https://doi.org/10.1115/1.2883725

[7] E. Kingston, M. Udagawa, J. Katsuyama, K. Onizawa, D.J. Smith, Measurement of residual stresses in stainless steel cladded specimens, Proceedings of the ASME Pressure Vessels and Piping Conference, 2010, p. 25315. https://doi.org/10.1115/PVP2010-25315

[8] N. Naveed, F. Hosseinzadeh, J. Kowal, Residual stress measurement in a stainless steel clad ferritic plate using the contour method, Proceedings of the ASME Pressure Vessels and Piping Conference, 2013, p. 97101. https://doi.org/10.1115/PVP2013-97101

[9] M.N. James, M. Newby, P. Doubell, D.G. Hattingh, K. Serasli, D.J. Smith, Weld residual stresses near the bimetallic interface in clad RPV steel: a comparison between deep-hole drilling and neutron diffraction data, Nucl. Eng. Des. 274 (2014) 56-65. https://doi.org/ 10.1016/j.nucengdes.2014.03.042

[10] K. Serasli, H. Coules, and D. J. Smith, Residual stresses in clad nuclear reactor pressure vessel steels; prediction, measurement and reconstruction, Proceedings of the ASME Pressure Vessels and Piping Conference, 2015, p. 45224. https://doi.org/10.1115/PVP2015-45224

[11] K. Serasli, Measurement and mapping of residual stresses in welded nuclear components, PhD Thesis, Department of Mechanical Engineering, University of Bristol, 2014.

[12] M. Udagawa, J. Katsuyama, K. Onizawa, Effects of residual stress by weld overlay cladding and PWHT on the structural integrity of RPV during PTS, Proceedings of the ASME Pressure Vessels and Piping Conference, 2007, p. 26556. https://doi.org/10.1115/PVP2007-26556

[13] J.F. Knott, Structural integrity of nuclear reactor pressure vessels, Philos. Mag. 93 (2013) 3835-3862. https://doi.org/10.1080/14786435.2013.815379

[14] R6: assessment of the integrity of structures containing defects, revision 4, amendment 11, EDF Energy, Gloucester, 2015.

[15] W.R. Corwin, R.G. Berggren, R.K. Nanstad, and R.J. Gray, Fracture behaviour of a neutron-irradiated stainless steel submerged arc weld cladding overlay, Nucl. Eng. Des. 89 (1) (1985) 199-221. https://doi.org/10.1016/0029-5493(85)90155-4

[16] G.C.M. Horne, Elastic follow-up and the interaction between applied and residual stresses, PhD Thesis, Department of Mechanical Engineering, University of Bristol, 2013.

[17] A. Turnbull, J.J. Pitts, J.D. Lord, Residual stress relaxation in shot peened high strength low alloy steel, Mater. Sci. Technol. 24 (3) (2013) 327-334. https://doi.org/10.1179/174328407x185776

[18] R. Bass, J. Wintle, R.C. Hurst, N. Taylor (Eds.), NESC-1 Project Overview, EUR 19051 EN, 2001.

[19] ASTM E8/E8M-15a Standard Test Methods for Tension Testing of Metallic Materials, ASTM International, West Conshohocken, 2015. https://doi.org/10.1520/e0008_e0008m-15a

[20] ASTM E837-13a Standard Test Method for Determining Residual Stresses by the Hole-Drilling Strain-Gage Method, ASTM International, West Conshohocken, 2013. https://doi.org/10.1520/e0837-13a

[21] R.H. Leggatt, D.J. Smith, S.D. Smith, F. Faure, Development and experimental validation of the deep hole method for residual stress measurement, J. Strain Anal. Eng. Des. 31 (3) (1996) 177-186. https://doi.org/10.1243/03093247v313177
[22] M. B. Prime, Cross-sectional mapping of residual stresses by measuring the surface contour after a cut, J Eng. Mater. Technol. 123 (2) (2001) 162-168. https://doi.org/10.1115/1.1345526
[23] D.B.F. George, Determination of residual stresses in large section stainless steel welds, PhD Thesis, Department of Mechanical Engineering, University of Bristol, 2000.
[24] M.F. Ashby, D.R.H. Jones, Engineering Materials 1, third ed., Elsevier, Oxford, 2005.
[25] Abaqus/CAE v6.14, Providence, RI, USA: Dassault Systemes Simulia Corp., 2014.
[26] R.F. Price, A.J. Fletcher, Determination of surface heat-transfer coefficients during quenching of steel plates, Met. Technol. 7 (1980) 203-211. https://doi.org/10.1179/030716980803286739
[27] A. Goldsmith, T.E. Waterman, H.J. Hirschhorn, Handbook of thermophysical properties of solid materials - Volume II: Alloys, Macmillan, New York, 1961.
[28] B.P. Bardes (Ed.), Metals handbook - Volume 1: Properties and selection: irons and steels, ninth ed., American Society for Metals, Ohio, 1978.
[29] Special Metals Corporation, INCONEL alloy 600 data sheet, SMC-027, http://www.specialmetals.com/assets/smc/documents/alloys/inconel/inconel-alloy-600.pdf, Sept. 2008 (accessed 1 August 2016).
[30] G. Panneerselvam, S. Raju, R. Jose, K. Sivasubramanian, R. Divakar, E. Mohandas, M.P. Antony, A study on the thermal expansion characteristics of Inconel-82® filler wire by high temperature X-ray diffraction, Mater. Lett. 58 (2004) 216-221. https://doi.org/10.1016/s0167-577x(03)00448-8
[31] W.J. Brayshaw (University of Manchester) SA508 Grade 4N tensile test data, unpublished raw data, 24 October 2016.
[32] B.A. Latella, S.R. Humphries, Young's modulus of a 2.25Cr–1Mo steel at elevated temperature, Scr. Mater. 51 (7) (2004) 635-639. https://doi.org/10.1016/j.scriptamat.2004.06.028
[33] G.V. Smith (Ed.), Evaluations of the elevated temperature tensile and creep-rupture properties of C-Mo, Mn-Mo and Mn-Mo-Ni steels, DS47-EB, ASTM International, West Conshohocken, PA, 1971. https://doi.org/10.1520/DS47-EB
[34] R.L. Klueh, J.F. King. Elevated temperature tensile behaviour of ERNiCr-3 weld metal. Welding Journal. (April 1980) 114-120.
[35] M.J. Marques, A. Ramasamy, A.C. Batista, J.P. Nobre, A. Loureiro, Effect of heat treatment on microstructure and residual stress fields of a weld

multilayer austenitic steel clad, J. Mater. Process. Technol. 222 (2015) 52-60. https://doi.org/10.1016/j.jmatprotec.2015.03.004
[36] E.F. Rybicki, J.R. Shadley, A.S. Sandhu, R.B. Stonesifer, Experimental and computational residual stress evaluation of a weld clad plate and machined test specimens, J. Eng. Mater. Technol. 110 (4) (1988) 297-304. https://doi.org/10.1115/1.3226053
[37] X.R. Wu, A.J. Carlsson, Weight functions and stress intensity factor solutions, first ed., Pergamon Press, Oxford, 1991.
[38] A. Mirzaee-Sisan, D. Smith, C. Truman, Characterizing residual stresses in rectangular beam specimens following thermomechanical loading, J. Strain Anal. Eng. Des. 42 (2) (2007) 79-93. https://doi.org/10.1243/03093247jsa215
[39] S. Hossain, C.E. Truman, D.J. Smith, M.R. Daymond, Application of quenching to create highly triaxial residual stresses in type 316H stainless steels, Int. J. Mech. Sci. 48 (3) (2006) 235-243. https://doi.org/10.1016/j.ijmecsci.2005.11.002